NeuroImage **16,** 269–282 (2002)
doi:10.1006/nimg.2001.1038, available online at http://www.idealibrary.com on IDEAL®

Analysis and Design of Perfusion-Based Event-Related fMRI Experiments

Thomas T. Liu,*[,1] Eric C. Wong,*[,†] Lawrence R. Frank,*[,‡] and Richard B. Buxton*

**Department of Radiology and †Department of Psychiatry, University of California at San Diego, La Jolla, California 92093; and ‡VA San Diego Healthcare System, San Diego, California 92161*

Received March 8, 2001

Perfusion-based functional magnetic resonance imaging (fMRI) using arterial spin labeling (ASL) methods has the potential to provide better localization of the functional signal to the sites of neural activity compared to blood oxygenation level-dependent (BOLD) contrast fMRI. At present, experiments using ASL have been limited to simple block and periodic single-trial designs. We present here an adaptation of the general linear model to perfusion-based fMRI that enables the design and analysis of more complicated designs, such as random and semirandom event-related designs. Formulas for the least-squares estimate of the perfusion response and the *F* statistic for the detection of a response are derived. Exact expressions and useful approximations for detection power and estimation efficiency are presented, and it is shown that the trade-off between power and efficiency for perfusion experiments is similar to that previously observed for BOLD experiments. The least-squares estimate is compared with an estimate formed from the running subtraction of tag and control images. The running subtraction estimate is shown to be approximately equal to a temporally low-pass-filtered version of the least-squares estimate. Numerical simulations and results from ASL experiments are used to support the theoretical findings. © 2002 Elsevier Science (USA)

Key Words: **fMRI; event-related; perfusion; arterial spin labeling.**

INTRODUCTION

Event-related experimental designs with random and semirandom interstimulus intervals have become increasingly popular for functional magnetic resonance imaging (fMRI) because they circumvent some of the problems, such as habituation, of more traditional block designs (Rosen *et al.*, 1998) and offer variable trade-offs between estimation efficiency and detection power (Dale, 1999; Friston *et al.*, 1999; Liu *et al.*, 2001a,b).

At present, the use of random and semirandom designs has been limited to experiments using blood oxygenation level-dependent (BOLD) contrast. Event-related experiments with perfusion-based fMRI using arterial spin labeling (ASL) have been reported, but have used periodic single-trial designs in which the events are widely spaced at regular intervals (Liu and Gao, 1999; Yang *et al.*, 2000). Recent improvements in the contrast-to-noise ratio and the temporal resolution of ASL techniques (Wong *et al.*, 2000), as well as the potential of ASL to better localize functional activation to neural activity (Duong *et al.*, 2000; Luh *et al.*, 2000), make the application of ASL techniques to the entire range of event-related designs increasingly attractive.

The design of event-related perfusion experiments is complicated by the fact that the perfusion image is formed from the difference between a control image in which the magnetization of arterial blood is fully relaxed and a tag image in which the magnetization of arterial blood is inverted. Typically, tag and control images are acquired in an interleaved fashion, reducing the temporal resolution of the experiment. To improve the effective temporal resolution for periodic single-trial designs, two strategies have been proposed: (a) acquire separate tag and control runs and (b) shift the timing of the stimulus with respect to that of the acquisition (Liu and Gao, 1999; Yang *et al.*, 2000). The first method cannot be applied to certain ASL sequences, such as turbo-PICORE (proximal inversion with control for off-resonance effects) tagging, in which the interleaving of tag and control images is an integral part of the technique (Wong *et al.*, 2000). In addition, the use of two separate runs may not be appropriate for cognitive experiments in which the response of the subject may vary from run to run. The extension of the second method to more complicated designs, such as randomized designs, is not obvious.

[1] To whom correspondence should be addressed at the Center for Functional Magnetic Resonance Imaging, 9500 Gilman Dr., MC 0677, La Jolla, CA 92093. Fax: (858) 657-6699. E-mail: ttliu@ucsd.edu.

1053-8119/02 $35.00

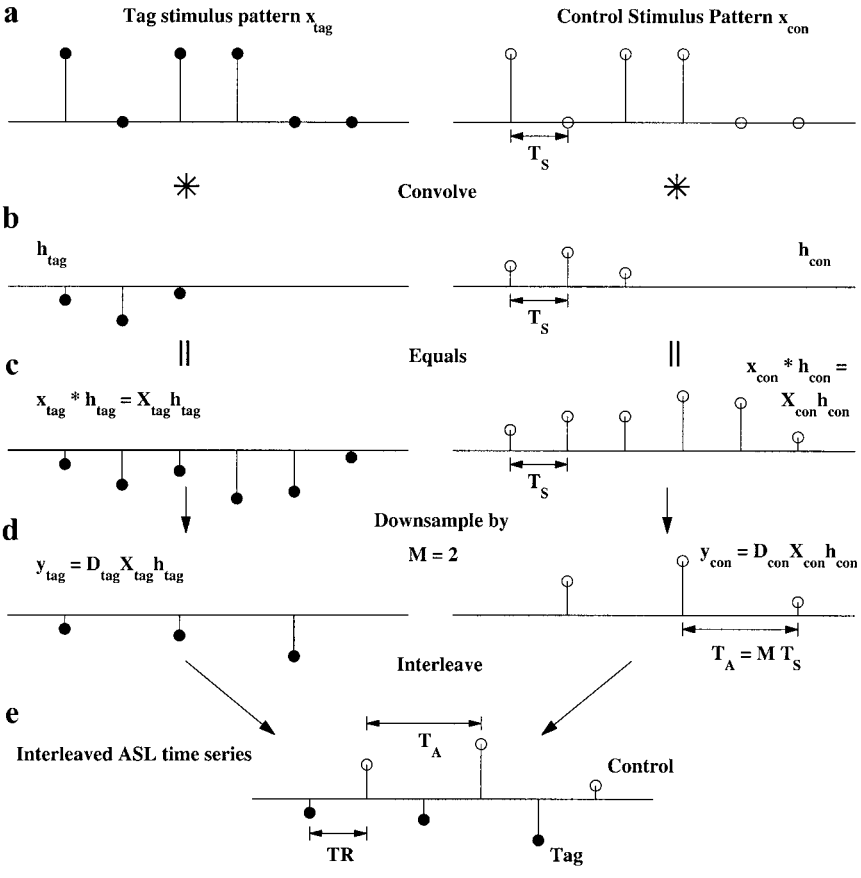

FIG. 1. Diagram showing the steps of convolution, downsampling, and interleaving in an ASL experiment.

In this paper, we present a framework for the design and analysis of perfusion fMRI experiments. This framework encompasses previously described methods and provides a means of analyzing and understanding the performance of perfusion fMRI experiments with any design that may be of interest. The structure of the paper is as follows. We first present a general linear model for perfusion fMRI experiments and then derive expressions for the least-squares estimate of the perfusion response and the *F* statistic for detection of a response. Next we derive exact and approximate expressions for the estimation efficiency and detection power of perfusion experiments and show that the trade-off between efficiency and power is similar to that previously reported for BOLD experiments (Liu *et al.*, 2001b). We also present a formal definition of perfusion estimates based upon a running subtraction of tag and control images. We show that the running subtraction estimate is approximately equal to a temporally low-pass-filtered version of the least-squares estimate and discuss the potential advantages of the running subtraction estimate. Results from numerical simulations and ASL experiments are used to validate the theoretical framework. Portions of this paper have been described in preliminary form (Liu *et al.*, 2001c).

THEORY

Basic Concepts

Experimental designs for perfusion imaging can be described with an extension of the general linear model (Friston *et al.*, 1995) commonly used in fMRI by making use of two observations. First, it is useful to treat the time series of tag images separately from the time series of control images. Second, the observed time series are typically acquired at a reduced sampling rate. For example, with interleaved tag and control images, the sampling rate of each series is reduced by a factor of 2 or more compared to a noninterleaved (e.g., BOLD) experiment.

To illustrate these observations, we outline in Fig. 1 the elements of an ASL experiment. In a typical ASL experiment, the tag and control images are interleaved as shown in Fig. 1e. The period between subsequent images is *TR*, the repetition time of the acquisition

pulse sequence. We denote the period between subsequent tag (or control) images as T_A, where for typical interleaved experiments, $T_A = 2TR$. We can think of forming the ASL time series by interleaving a tag time series $\mathbf{y}_{tag}$ with a control time series $\mathbf{y}_{con}$, both shown in Fig. 1d.

We next examine how $\mathbf{y}_{tag}$ and $\mathbf{y}_{con}$ are formed and will find it useful to consider for a moment the measured responses from a noninterleaved ASL experiment (e.g., Liu and Gao, 1999) in which there are separate tag and control runs. With the assumption of a general linear model, the measured response during each run, ignoring constant terms and low-frequency confounds, is given by the convolution of the stimulus pattern and the hemodynamic response. Thus, the response during the tag condition is given by $\mathbf{x}_{tag} * \mathbf{h}_{tag}$, where $*$ denotes convolution and $\mathbf{x}_{tag}$ and $\mathbf{h}_{tag}$ are the tag stimulus pattern and hemodynamic response, respectively. Similarly, the response during the control condition is given by $\mathbf{x}_{con} * \mathbf{h}_{con}$. Examples of these sequences are shown in Figs. 1a, 1b, and 1c, where both $\mathbf{x}_{tag}$ and $\mathbf{x}_{con}$ are equal to the 6-element binary sequence [1, 0, 1, 1, 0, 0] and both $\mathbf{h}_{tag}$ and $\mathbf{h}_{con}$ are 3-element sequences. We define T_S as the time between the elements in the stimulus pattern. This period determines the time resolution of the experiment, for both interleaved and noninterleaved cases, meaning that estimates of the hemodynamic response will have a temporal resolution equal to T_S. In preparation for the general linear model framework, we rewrite the convolution products as matrix multiplication products, such that $\mathbf{x}_{tag} * \mathbf{h}_{tag} = \mathbf{X}_{tag}\mathbf{h}_{tag}$ and $\mathbf{x}_{con} * \mathbf{h}_{con} = \mathbf{X}_{con}\mathbf{h}_{con}$, where $\mathbf{X}_{tag}$ and $\mathbf{X}_{con}$ are design matrices whose columns are formed from shifted versions of $\mathbf{x}_{tag}$ and $\mathbf{x}_{con}$, respectively (Dale, 1999).

In a noninterleaved ASL experiment, we measure all the data points in $\mathbf{X}_{tag}\mathbf{h}_{tag}$ and $\mathbf{X}_{con}\mathbf{h}_{con}$, usually in separate runs. By contrast, for an interleaved ASL experiment, we measure a subset of the data points because we alternate between measuring a point from $\mathbf{X}_{tag}\mathbf{h}_{tag}$ and a point from $\mathbf{X}_{con}\mathbf{h}_{con}$. Thus, as shown in Figs. 1c and 1d, the series of tag images $\mathbf{y}_{tag}$ consists of every even sample of $\mathbf{X}_{tag}\mathbf{h}_{tag}$, while the series of control images $\mathbf{y}_{con}$ consists of every odd sample of $\mathbf{X}_{con}\mathbf{h}_{con}$. This process is referred to as downsampling and can be compactly described through the use of downsampling matrices $\mathbf{D}_{tag}$ and $\mathbf{D}_{con}$, such that $\mathbf{y}_{tag} = \mathbf{D}_{tag}\mathbf{X}_{tag}\mathbf{h}_{tag}$ and $\mathbf{y}_{con} = \mathbf{D}_{con}\mathbf{X}_{con}\mathbf{h}_{con}$ (Strang and Nguyen, 1997). For the example shown, $\mathbf{D}_{tag}$ is a matrix which picks out every even sample of $\mathbf{X}_{tag}\mathbf{h}_{tag}$ and $\mathbf{D}_{con}$ is a matrix which picks out every odd sample of $\mathbf{X}_{tag}\mathbf{h}_{tag}$. To further clarify how the convolution and downsampling operations work, we expand the matrix expressions for $\mathbf{y}_{tag}$ and $\mathbf{y}_{con}$ using the stimulus patterns shown in Fig. 1. The expressions are as follows:

$$
\begin{aligned}
\mathbf{y}_{tag} &= \mathbf{D}_{tag}\mathbf{X}\mathbf{h}_{tag} \\
&= \begin{bmatrix} 1 & 0 & 0 & 0 & 0 & 0 \\ 0 & 0 & 1 & 0 & 0 & 0 \\ 0 & 0 & 0 & 0 & 1 & 0 \end{bmatrix} \begin{bmatrix} 1 & 0 & 0 \\ 0 & 1 & 0 \\ 1 & 0 & 1 \\ 1 & 1 & 0 \\ 0 & 1 & 1 \\ 0 & 0 & 1 \end{bmatrix} \begin{bmatrix} h_{tag,1} \\ h_{tag,2} \\ h_{tag,3} \end{bmatrix} \\
&= \begin{bmatrix} h_{tag,1} \\ h_{tag,1} + h_{tag,3} \\ h_{tag,2} + h_{tag,3} \end{bmatrix}, \\
\mathbf{y}_{con} &= \mathbf{D}_{con}\mathbf{X}\mathbf{h}_{con} \\
&= \begin{bmatrix} 0 & 1 & 0 & 0 & 0 & 0 \\ 0 & 0 & 0 & 1 & 0 & 0 \\ 0 & 0 & 0 & 0 & 0 & 1 \end{bmatrix} \begin{bmatrix} 1 & 0 & 0 \\ 0 & 1 & 0 \\ 1 & 0 & 1 \\ 1 & 1 & 0 \\ 0 & 1 & 1 \\ 0 & 0 & 1 \end{bmatrix} \begin{bmatrix} h_{con,1} \\ h_{con,2} \\ h_{con,3} \end{bmatrix} \\
&= \begin{bmatrix} h_{con,1} \\ h_{con,1} + h_{con,2} \\ h_{con,3} \end{bmatrix}.
\end{aligned}
\tag{1}
$$

In general, downsampling can be used to pick out every Mth sample of a time series, where M is defined as the downsampling factor. In the example shown in Fig. 1, M is equal to 2. The sampling period T_A of the downsampled time series is related to the period T_S of the stimulus pattern by the equation $T_A = MT_S$. In this paper we assume that M is an integer that is greater than or equal to 1. The use of noninteger downsampling factors is addressed under Discussion and Conclusion.

To demonstrate the use of downsampling in practice, we consider three types of ASL experiments with downsampling factors ranging in value from 1 to 4. We assume in each case that the stimulus pattern is defined on a 1-s time grid, i.e., T_S is 1 s. $M = 1$ example: Nonquantitative ASL data are acquired in a noninterleaved fashion with a close-tag continuous arterial spin labeling (CASL) sequence (Wong *et al.*, 2001) with a TR of 1 s. That is, a series of tag images is followed by a series of control images. In this case $T_A = 1$ s and $\mathbf{D}_{tag}$ and $\mathbf{D}_{con}$ are both identity matrices. $M = 2$ example: ASL data are acquired in an interleaved fashion with a turbo-PICORE sequence (Wong *et al.*, 2000) at a TR of 1 s. In this case $T_A = 2$ s. $M = 4$ example: ASL data are acquired in an interleaved fashion with a FAIR, EPISTAR, or PICORE sequence (Wong *et al.*, 1997) at a TR of 2 s. In this case $T_A = 4$ s. These examples are summarized in Table 1.

General Linear Model

Equation (1) captures the essence of the ASL experiment. In the absence of noise and other confounds, we can directly compute $\mathbf{h}_{tag}$ and $\mathbf{h}_{con}$ from the observed time series $\mathbf{y}_{tag}$ and $\mathbf{y}_{con}$, provided the matrices $\mathbf{D}_{tag}\mathbf{X}_{tag}$

TABLE 1

Examples of Downsampling in ASL Experiments

Method	TR (s)	T_A (s)	M	$\mathbf{D}_{tag}$	$\mathbf{D}_{con}$
Noninterleaved close-tag CASL	1	1	1	$\begin{bmatrix}1 & 0\\ 0 & 1\end{bmatrix}$	$\begin{bmatrix}1 & 0\\ 0 & 1\end{bmatrix}$
Turbo-PICORE	1	2	2	$\begin{bmatrix}1 & 0 & 0 & 0\\ 0 & 0 & 1 & 0\end{bmatrix}$	$\begin{bmatrix}0 & 1 & 0 & 0\\ 0 & 0 & 0 & 1\end{bmatrix}$
FAIR, EPISTAR, or PICORE	2	4	4	$\begin{bmatrix}1 & 0 & 0 & 0 & 0 & 0 & 0 & 0\\ 0 & 0 & 0 & 0 & 1 & 0 & 0 & 0\end{bmatrix}$	$\begin{bmatrix}0 & 0 & 1 & 0 & 0 & 0 & 0 & 0\\ 0 & 0 & 0 & 0 & 0 & 0 & 1 & 0\end{bmatrix}$

Note. For all examples, the sample period T_S of the stimulus pattern is assumed to be 1 s and the dimension p of the observed time series is equal to 2. The dimensions of the stimulus patterns are $N = 2$, 4, and 8 for CASL, turbo-PICORE, and FAIR (also EPISTAR or PICORE), respectively.

and $\mathbf{D}_{con}\mathbf{X}_{con}$ have full rank. To obtain a general linear model, we add terms for noise and other confounds, such that

$$\begin{bmatrix}\mathbf{y}_{tag}\\ \mathbf{y}_{con}\end{bmatrix} = \begin{bmatrix}\mathbf{D}_{tag}\mathbf{X}_{tag} & \mathbf{0}_{p\times k}\\ \mathbf{0}_{p\times k} & \mathbf{D}_{con}\mathbf{X}_{con}\end{bmatrix}\begin{bmatrix}\mathbf{h}_{tag}\\ \mathbf{h}_{con}\end{bmatrix} + \begin{bmatrix}\mathbf{S}_{tag} & \mathbf{0}_{p\times l}\\ \mathbf{0}_{p\times l} & \mathbf{S}_{con}\end{bmatrix}\begin{bmatrix}\mathbf{b}_{tag}\\ \mathbf{b}_{con}\end{bmatrix} + \mathbf{n}, \tag{2}$$

where $\mathbf{y}_{tag}$ and $\mathbf{y}_{con}$ are $p \times 1$ vectors that represent the observed tag and control time series, respectively, $\mathbf{X}_{tag}$ and $\mathbf{X}_{con}$ are $N \times k$ design matrices, $\mathbf{h}_{tag}$ and $\mathbf{h}_{con}$ are $k \times 1$ parameter vectors, $\mathbf{D}_{tag}$ and $\mathbf{D}_{con}$ are $p \times N$ downsampling matrices, $\mathbf{S}_{tag}$ and $\mathbf{S}_{con}$ are $p \times l$ matrices consisting of nuisance model functions, $\mathbf{b}_{tag}$ and $\mathbf{b}_{con}$ are $l \times 1$ vectors of nuisance parameters, and $\mathbf{n}$ is a $2p \times 1$ vector that represents additive Gaussian noise. The notation $\mathbf{0}_{p\times k}$ indicates a $p \times k$ matrix of zeros. We define the dimension p as $p = N/M$, where M is the downsampling factor defined above. For ASL experiments in which tag and control images are interleaved we require that $\mathbf{X}_{tag}$ be identical to $\mathbf{X}_{con}$, and we define the common design matrix as $\mathbf{X} = \mathbf{X}_{tag} = \mathbf{X}_{con}$; for noninterleaved experiments, such as those described in Liu and Gao (1999), there is no such restriction. We assume that the covariance of the noise vector $\mathbf{n}$ is given by $\mathbf{C}_{\mathbf{n}} = \sigma^2\mathbf{I}$, where $\mathbf{I}$ is the identity matrix and σ^2 is an unknown variance term that needs to be estimated from the data.

The terms $\mathbf{S}_{tag}\mathbf{b}_{tag}$ and $\mathbf{S}_{con}\mathbf{b}_{con}$ in the linear model represent nuisance terms such as a constant term, a linear trend, and other low-frequency drifts. The parameter values associated with the constant terms are of interest for determining the baseline perfusion value, while the parameters associated with the other nuisance terms are typically of no interest.

To simplify the presentation in the remainder of the paper, we derive theoretical expressions using a simplified model in which $\mathbf{X} = \mathbf{X}_{tag} = \mathbf{X}_{con}$ and $\mathbf{S} = \mathbf{S}_{tag} = \mathbf{S}_{con}$ so that

$$\begin{bmatrix}\mathbf{y}_{tag}\\ \mathbf{y}_{con}\end{bmatrix} = \begin{bmatrix}\mathbf{D}_{tag}\mathbf{X} & \mathbf{0}_{p\times k}\\ \mathbf{0}_{p\times k} & \mathbf{D}_{con}\mathbf{X}\end{bmatrix}\begin{bmatrix}\mathbf{h}_{tag}\\ \mathbf{h}_{con}\end{bmatrix} + \begin{bmatrix}\mathbf{S} & \mathbf{0}_{p\times l}\\ \mathbf{0}_{p\times l} & \mathbf{S}\end{bmatrix}\begin{bmatrix}\mathbf{b}_{tag}\\ \mathbf{b}_{con}\end{bmatrix} + \mathbf{n}. \tag{3}$$

The expressions we derive for the simplified model are easily modified to handle the more general model by simply replacing $\mathbf{X}$ with $\mathbf{X}_{tag}$ and $\mathbf{S}$ with $\mathbf{S}_{tag}$ whenever $\mathbf{X}$ or $\mathbf{S}$ appears next to $\mathbf{D}_{tag}$ and applying a similar transformation for $\mathbf{X}_{con}$ and $\mathbf{S}_{con}$. Following Liu *et al.* (2001b), we refer to the subspaces spanned by the columns of $\mathbf{X}$ and $\mathbf{S}$ as the signal subspace $\langle\mathbf{X}\rangle$ and the interference subspace $\langle\mathbf{S}\rangle$, respectively. Note that this is a slight abuse of notation since the signal subspaces of $\mathbf{y}_{tag}$ and $\mathbf{y}_{con}$ are spanned by the columns of $\mathbf{D}_{tag}\mathbf{X}$ and $\mathbf{D}_{con}\mathbf{X}$, respectively. We require $\langle\mathbf{X}\rangle$ and $\langle\mathbf{S}\rangle$ to be linearly independent but not necessarily orthogonal.

Estimation

Using the theory of oblique projections described in Behrens and Scharf (1994), we may write the maximum likelihood estimates of the tag and control hemodynamic responses as

$$\begin{aligned}\hat{\mathbf{h}}_{tag} &= (\mathbf{X}^T\mathbf{D}_{tag}^T\mathbf{P}_{\mathbf{S}}^{\perp}\mathbf{D}_{tag}\mathbf{X})^{-1}\mathbf{X}^T\mathbf{D}_{tag}^T\mathbf{P}_{\mathbf{S}}^{\perp}\mathbf{y}_{tag},\\ \hat{\mathbf{h}}_{con} &= (\mathbf{X}^T\mathbf{D}_{con}^T\mathbf{P}_{\mathbf{S}}^{\perp}\mathbf{D}_{con}\mathbf{X})^{-1}\mathbf{X}^T\mathbf{D}_{con}^T\mathbf{P}_{\mathbf{S}}^{\perp}\mathbf{y}_{con},\end{aligned} \tag{4}$$

where $\mathbf{P}_{\mathbf{S}}^{\perp} = \mathbf{I} - \mathbf{S}(\mathbf{S}^T\mathbf{S})^{-1}\mathbf{S}^T$ is a projection matrix that removes the part of a vector that lies in the interference subspace $\langle\mathbf{S}\rangle$. Note that in order for the estimates to exist, the inverses $(\mathbf{X}^T\mathbf{D}_{tag}^T\mathbf{P}_{\mathbf{S}}^{\perp}\mathbf{D}_{tag}\mathbf{X})^{-1}$ and $(\mathbf{X}^T\mathbf{D}_{con}^T\mathbf{P}_{\mathbf{S}}^{\perp}\mathbf{D}_{con}\mathbf{X})^{-1}$ must exist or equivalently $\mathbf{P}_{\mathbf{S}}^{\perp}\mathbf{D}_{tag}\mathbf{X}$ and $\mathbf{P}_{\mathbf{S}}^{\perp}\mathbf{D}_{con}\mathbf{X}$ must have full rank. When M is greater than 1, a sufficient, but not necessary, condition for rank deficiency is for the events, i.e., 1's in the stimulus pattern, to be constrained to lie on a time grid with a spacing of $T_A/m = MT_S/m$, where m is the largest integer value less than $M - 1$ for which M/m is an

integer. As an example, if $M = 4$, $T_A = 4$ s, and $T_S = 1$ s, then $m = 2$ is the largest integer less than $M - 1 = 3$ for which M/m is an integer, and $T_A/m = 2$ s. Thus, the inverses will fail to exist if the events in the stimulus pattern are constrained to occur at times that are multiples of 2 s, e.g., the inverses do not exist for a periodic design with $T_S = 1$ s in which there is a 1 in the binary stimulus pattern every 20 s, with all other elements of the pattern being set to zero. This design can be modified to avoid rank deficiency in the following ways. If the spacing between events is required to be uniform for the entire experiment than the spacing can be set to an odd number of seconds (e.g., an event every 21 s) as was done in Miller *et al.* (2000). If the spacing between events is required to be an even number of seconds, then stimulus shifting can be used at certain points within a run (Liu and Gao, 1999) or across runs (Yang *et al.*, 2000) to move the events off the 2-s time grid, e.g., a spacing of 20 s between events, except for a spacing of 21 s between two consecutive events at a point approximately halfway through the run. Note that the condition stated above is a sufficient but not necessary condition—i.e., there exist full rank design matrices $\mathbf{X}$ that do not satisfy the condition, but nevertheless have rank deficient $\mathbf{P}_{\mathbf{S}}^{\perp}\mathbf{D}_{tag}\mathbf{X}$ and $\mathbf{P}_{\mathbf{S}}^{\perp}\mathbf{D}_{con}\mathbf{X}$.

An estimate of the perfusion response can be formed from the difference of $\hat{\mathbf{h}}_{con}$ and $\hat{\mathbf{h}}_{tag}$. In addition, for most pulsed ASL techniques the sum of $\hat{\mathbf{h}}_{con}$ and $\hat{\mathbf{h}}_{tag}$ yields an estimate of the BOLD response (Wong *et al.*, 1997). That is,

$$\begin{aligned}\hat{\mathbf{h}}_{perf} &= \hat{\mathbf{h}}_{con} - \hat{\mathbf{h}}_{tag},\\ \hat{\mathbf{h}}_{BOLD} &= \hat{\mathbf{h}}_{con} + \hat{\mathbf{h}}_{tag}.\end{aligned} \tag{5}$$

For periodic single-trial designs, these estimates are analogous to those previously reported in the literature (Liu and Gao, 1999; Yang *et al.*, 2000). The covariance matrix for both estimates is given by $\mathbf{C}_{\hat{\mathbf{h}}_{perf}} = \mathbf{C}_{\hat{\mathbf{h}}_{BOLD}} = \sigma^2(\mathbf{X}^T\mathbf{D}_{tag}^T\mathbf{P}_{\mathbf{S}}^{\perp}\mathbf{D}_{tag}\mathbf{X})^{-1} + \sigma^2(\mathbf{X}^T\mathbf{D}_{con}^T\mathbf{P}_{\mathbf{S}}^{\perp}\mathbf{D}_{con}\mathbf{X})^{-1}$ and may be used to evaluate the estimation efficiency, a measure of the ability of a design to characterize the hemodynamic response. A useful definition of efficiency is the inverse of the sum of the variances of the components of $\hat{\mathbf{h}}_{perf}$ (Seber, 1977; Dale, 1999),

$$\xi = \frac{1}{Trace[\mathbf{C}_{\hat{\mathbf{h}}_{perf}}]} = \frac{1}{\sigma^2 Trace[(\mathbf{X}^T\mathbf{D}_{tag}^T\mathbf{P}_{\mathbf{S}}^{\perp}\mathbf{D}_{tag}\mathbf{X})^{-1} + (\mathbf{X}^T\mathbf{D}_{con}^T\mathbf{P}_{\mathbf{S}}^{\perp}\mathbf{D}_{con}\mathbf{X})^{-1}]}. \tag{6}$$

Detection

Detection refers to the problem of deciding if a perfusion response occurred. It can be formally stated as the test of the null hypothesis $\hat{\mathbf{h}}_{perf} = 0$. To derive the statistic used to test this hypothesis, we rewrite the simplified model of Eq. (3) in the form $\mathbf{y} = \mathbf{Z}\beta + \mathbf{n}$, where

$$\mathbf{y} = \begin{bmatrix}\mathbf{y}_{tag}\\ \mathbf{y}_{con}\end{bmatrix},\ \beta = \begin{bmatrix}\mathbf{h}_{tag}\\ \mathbf{h}_{con}\\ \mathbf{b}_{tag}\\ \mathbf{b}_{con}\end{bmatrix},\qquad \mathbf{Z} = \begin{bmatrix}\mathbf{D}_{tag}\mathbf{X} & \mathbf{0}_{p\times k} & \mathbf{S} & \mathbf{0}_{p\times l}\\ \mathbf{0}_{p\times k} & \mathbf{D}_{con}\mathbf{X} & \mathbf{0}_{p\times l} & \mathbf{S}\end{bmatrix}. \tag{7}$$

The hypothesis $\hat{\mathbf{h}}_{perf} = 0$ is then equivalent to the hypothesis that $\mathbf{A}\beta = \mathbf{0}$ where $\mathbf{A} = [-\mathbf{I}_{k\times k}\ \mathbf{I}_{k\times k}\ \mathbf{0}_{k\times 2l}]$ and $\mathbf{I}_{k\times k}$ is the $k \times k$ identity matrix. The F statistic for testing this hypothesis has the form

$$F = \frac{(2p - 2k - 2l)}{k}\,\frac{\hat{\beta}^T\mathbf{A}^T[\mathbf{A}(\mathbf{Z}^T\mathbf{Z})^{-1}\mathbf{A}^T]^{-1}\mathbf{A}\hat{\beta}}{RSS}, \tag{8}$$

where $RSS = (\mathbf{y} - \mathbf{Z}\hat{\beta})^T(\mathbf{y} - \mathbf{Z}\hat{\beta})$ is the residual sum of squares for the full model and $\hat{\beta} = (\mathbf{Z}^T\mathbf{Z})^{-1}\mathbf{Z}^T\mathbf{y}$ (Seber, 1977). If F is below a certain threshold, we accept the hypothesis $\hat{\mathbf{h}}_{perf} = 0$ and conclude that there was no perfusion response; otherwise, we reject the hypothesis and conclude that a perfusion response occurred. Substituting for $\mathbf{A}$, $\mathbf{Z}$, and β, we may rewrite the F statistic as

$$F = \frac{(2p - 2k - 2l)}{k}\,\frac{\hat{\mathbf{h}}_{perf}^T[(\mathbf{X}^T\mathbf{D}_{tag}^T\mathbf{P}_{\mathbf{S}}^{\perp}\mathbf{D}_{tag}\mathbf{X})^{-1} + (\mathbf{X}^T\mathbf{D}_{con}^T\mathbf{P}_{\mathbf{S}}^{\perp}\mathbf{D}_{con}\mathbf{X})^{-1}]^{-1}\hat{\mathbf{h}}_{perf}}{RSS}. \tag{9}$$

Detection power is a measure of the ability of a design to detect an activation (Liu *et al.*, 2001b). Formally, it is the probability that we detect a perfusion response when a perfusion response is actually present. When a response is present, the F statistic follows a noncentral F distribution with noncentrality parameter (Scharf, 1991).

$$\eta = \mathbf{h}_{perf}^T\mathbf{C}_{\hat{\mathbf{h}}_{perf}}^{-1}\mathbf{h}_{perf}/\sigma^2. \tag{10}$$

For a given threshold on the F statistic, the detection power (i.e., the integral of the noncentral F distribution for values above the threshold) increases with the noncentrality parameter. Thus, the noncentrality parameter serves as a useful metric for the detection power of a design. As shown in Liu *et al.* (2001b), it is useful to normalize the noncentrality parameter by the energy

$\mathbf{h}_{perf}^T \mathbf{h}_{perf}$ of the parameter vector to obtain the Rayleigh quotient

$$R = \frac{\mathbf{h}_{perf}^T \mathbf{C}_{\hat{\mathbf{h}}_{perf}}^{-1} \mathbf{h}_{perf}}{\sigma^2 \mathbf{h}_{perf}^T \mathbf{h}_{perf}}, \quad (11)$$

which will serve as the metric for detection power for the remainder of the paper.

Performance of Designs

All experimental designs offer a trade-off between estimation efficiency and detection power. As shown in Liu *et al.* (2001b), this trade-off is fundamental because it depends on the distribution of the eigenvalues of $\mathbf{C}_{\hat{\mathbf{h}}_{perf}}^{-1}$. Estimation efficiency is maximized when the eigenvalues are equal, while detection power is maximized when one eigenvalue is dominant.

To gain further insight into the trade-off between efficiency and power for perfusion experiments it is useful to introduce the approximations

$$\mathbf{X}^T \mathbf{D}_{con}^T \mathbf{P}_{\tilde{\mathbf{S}}}^{\perp} \mathbf{D}_{con} \mathbf{X} \approx \mathbf{X}^T \mathbf{D}_{tag}^T \mathbf{P}_{\tilde{\mathbf{S}}}^{\perp} \mathbf{D}_{tag} \mathbf{X} \approx \frac{1}{M} \mathbf{X}_{\perp}^T \mathbf{X}_{\perp}, \quad (12)$$

where $\mathbf{X}_{\perp} = \mathbf{P}_{\tilde{\mathbf{S}}}^{\perp} \mathbf{X}$ is the design matrix with constant and nuisance terms removed from each column, $\tilde{\mathbf{S}}$ is the $N \times l$ matrix with nuisance model functions such that $\mathbf{S} \approx \mathbf{D}_{tag} \tilde{\mathbf{S}} \approx \mathbf{D}_{con} \tilde{\mathbf{S}}$, and $\mathbf{P}_{\tilde{\mathbf{S}}}^{\perp} = \mathbf{I} - \tilde{\mathbf{S}}(\tilde{\mathbf{S}}^T \tilde{\mathbf{S}})^{-1} \tilde{\mathbf{S}}^T$. These approximations are valid when the columns of $\mathbf{X}$ consist of shifted binary stimulus patterns and reflect the fact that $\mathbf{D}_{tag}$ picks out approximately $1/M$ of the 1's in the stimulus pattern while $\mathbf{D}_{con}$ picks out the other half. Under certain conditions (e.g., a periodic single-trial design and $\mathbf{S}$ consisting of only a constant term) the approximation becomes an equality.

Using the approximations in Eq. (12) and assuming unit noise variance leads to the following approximate expressions for estimation efficiency and Rayleigh quotient:

$$\xi \approx \frac{\kappa}{2M} \frac{1}{Trace[(\mathbf{X}_{\perp}^T \mathbf{X}_{\perp})^{-1}]}, \quad \mathbf{R} \approx \frac{\kappa}{2M} \frac{\mathbf{h}_{perf}^T \mathbf{X}_{\perp}^T \mathbf{X}_{\perp} \mathbf{h}_{perf}}{\mathbf{h}_{perf}^T \mathbf{h}_{perf}}. \quad (13)$$

Note that the assumption of unit variance for the noise-normalized expressions is valid because the noise variance enters as the same scaling factor of $1/\sigma^2$ in both Eqs. (6) and (11) and therefore does not change the relation between the efficiency and the Rayleigh quotient. Aside from the factor of $\kappa/(2M)$, these expressions are identical in form to those for the efficiency and Rayleigh quotient of a BOLD contrast experiment with design matrix $\mathbf{X}$ (Liu *et al.*, 2001b). The scaling factor κ is determined empirically by comparing the expressions in Eq. (13) with those in Eqs. (6) and (11). The introduction of this empirical scaling factor is necessary because approximation errors in Eq. (12) are amplified when computing the matrix inverses of each of the terms for use in Eqs. (6), (11), and (13). For most designs, κ ranges from 0.7 to 1.0 for $M = 2$ and from 0.5 to 1.0 for $M = 4$, with $\kappa = 1$ corresponding to the case in which the approximations in Eq. (12) become equalities (e.g., periodic single-trial design).

Because the approximate expressions for estimation efficiency and Rayleigh quotient are identical in form to those previously derived for BOLD experiments, the theory describing the performance of BOLD experiments (Liu *et al.*, 2001b) also provides insight into the performance of perfusion experiments. In short, randomized designs achieve optimal estimation efficiency but relatively poor detection power, whereas block designs maximize detection power at the cost of minimal estimation efficiency. Semirandom designs that lie between randomized and block designs offer intermediate trade-offs between efficiency and power.

To illustrate the performance of designs and the validity of the approximations in Eq. (13), we calculated the efficiencies and Rayleigh quotients for eight experimental designs ranging from a block design to a randomized design. Each design consisted of 128 time points with 64 events. The block design consisted of four on/off cycles and the semirandom designs were obtained by randomly permuting this block design (Buxton *et al.*, 2000). The randomized design was obtained by generating 1000 patterns with a uniform distribution of 1's and selecting the pattern that provided the greatest estimation efficiency for the BOLD experiment. The dimension of the perfusion response was $k = 15$, and the interference subspace consisted of only a constant term (i.e., $l = 1$). For computation of the Rayleigh quotient, $\mathbf{h}_{perf}$ was a gamma density function of the form

$$h[j] == C \cdot (\tau n!)^{-1} (j\Delta t/\tau)^n \exp(-j\Delta t/\tau), \quad (14)$$

where $C = 1$, $\tau = 1.2$, $n = 3$, and $\Delta t = 1$. For each design, the efficiencies and Rayleigh quotients of perfusion experiments with $M = 2$ and $M = 4$ were computed using the expressions in Eqs. (6) and (11). In addition the efficiency and Rayleigh quotient of the BOLD experiment were computed using the expression in Eq. (13) and omitting the factor of $\kappa/(2M)$.

Figure 2 shows calculated estimation efficiencies and Rayleigh quotients for perfusion and BOLD experiments. For comparison with the BOLD efficiency and Rayleigh quotient, the perfusion metrics are scaled by $2M/\kappa$ with $\kappa = 1$ for the block design and κ equal to 0.83

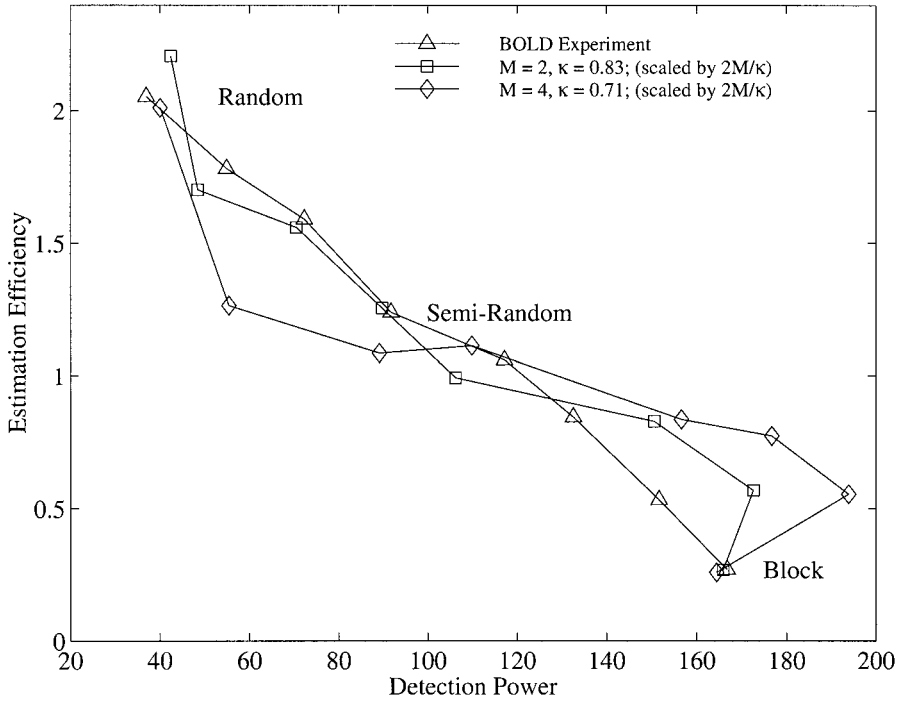

FIG. 2. Trade-off between estimation efficiency and detection power (Rayleigh quotient) for BOLD experiments and perfusion experiments with $M = 2$ and $M = 4$. Efficiency and power for perfusion experiments are scaled as indicated in the legend, except that $\kappa = 1$ for the block design. Unit noise variance is assumed.

and 0.71 for $M = 2$ and $M = 4$, respectively, for the other designs. The values of κ for the nonblock designs were chosen empirically to provide the best fit between the BOLD and the perfusion metrics. The agreement between the BOLD and the scaled perfusion metrics is fairly good and demonstrates the validity of the approximate expressions in Eq. (13). The fundamental trade-off between estimation efficiency and detection power is apparent for both BOLD and perfusion experimental designs.

It is important to point out that Fig. 2 does not imply that, after taking into account the factor of $\kappa/(2M)$, the actual estimation efficiency and detection power of a BOLD experiment are approximately the same as the efficiency and power of a perfusion experiment. In fact, the BOLD and perfusion metrics may differ significantly because of both differences in the shapes and amplitudes of the BOLD and perfusion hemodynamic responses and differences in the noise characteristics of the BOLD and ASL experiments. The simulation results do not reflect these potential differences because they were computed using normalizations and assumptions that were useful for demonstrating the fundamental trade-off between efficiency and power. Specifically, the normalized metrics stated in Eq. (13) assume unit noise variance, and the presence of the denominator term in the Rayleigh quotient normalizes for differences in the hemodynamic response amplitudes. In addition, the same shape for the BOLD and perfusion hemodynamic responses was assumed.

Covariance of Perfusion and BOLD Estimates

In ASL experiments in which both perfusion and BOLD estimates are formed, it is of interest to examine the covariance between the two estimates. This is given by the expression

$$\begin{aligned}\mathbf{C}_{\hat{\mathbf{h}}_{BOLD},\hat{\mathbf{h}}_{perf}} &= E[(\hat{\mathbf{h}}_{BOLD} - E[\hat{\mathbf{h}}_{BOLD}])(\hat{\mathbf{h}}_{perf} - E[\hat{\mathbf{h}}_{perf}])^T] \\ &= \sigma^2(\mathbf{X}^T\mathbf{D}_{con}^T\mathbf{P}_{\mathbf{S}}^{\perp}\mathbf{D}_{con}\mathbf{X})^{-1} - \sigma^2(\mathbf{X}^T\mathbf{D}_{tag}^T\mathbf{P}_{\mathbf{S}}^{\perp}\mathbf{D}_{tag}\mathbf{X})^{-1},\end{aligned} \tag{15}$$

where $E[\cdot]$ denotes expectation. Using the approximation stated in Eq. (12), we find that the covariance between the estimates is approximately zero for most designs and is identically zero for designs (e.g., periodic single trial) for which Eq. (12) is an equality. It is important to note that Eq. (15) is the statistical correlation between the random errors in the perfusion and the BOLD estimates and does not provide information about systematic errors that reflect the physics of the ASL experiment. In practice, the perfusion estimate will tend to be higher than the actual perfusion response due to BOLD contrast weighting of the tag and control images, and the BOLD estimate will tend to be

lower than the actual BOLD response due to the effect of inflowing magnetic spins (Wong *et al.*, 1997). These effects can be minimized by using short echo times in the imaging sequence and by applying an in-plane presaturation pulse prior to the tag and control pulses.

Running Subtraction Estimates

Perfusion experiments with block designs have typically used a running subtraction of the tag and control images to form a time series of perfusion images. The subtraction may be either a pairwise difference of adjacent tag and control images or the difference of each image from the average of the previous image and the next image (Wong *et al.*, 1997). Running subtraction approaches have the advantage of significantly reducing the effects of low-frequency drifts and motion-related artifacts. However, the applicability of a running subtraction type approach to event-related perfusion experiments has been questioned (Liu and Gao, 1999; Yang *et al.*, 2000). Here we present a formal definition of the running subtraction approach and examine the applicability of the approach to event-related perfusion experiments.

The running subtraction approach is equivalent to separately interpolating the tag and control time series to the desired time resolution and then forming the difference of the interpolated time series. That is, we first form the interpolated time series $\tilde{\mathbf{y}}_{tag} = \mathbf{G}\mathbf{U}_{tag}\mathbf{y}_{tag}$ and $\tilde{\mathbf{y}}_{con} = \mathbf{G}\mathbf{U}_{con}\mathbf{y}_{con}$, where $\tilde{\mathbf{y}}_{tag}$ and $\tilde{\mathbf{y}}_{con}$ are both $N \times 1$ vectors, $\mathbf{U}_{tag}$ and $\mathbf{U}_{con}$ are $N \times p$ matrices that upsample by a factor of M, and $\mathbf{G}$ is a $N \times N$ low-pass-filtering matrix. For example, with $M = 2$ and $N = 4$, we would have

$$\mathbf{U}_{tag} = \begin{bmatrix} 1 & 0 \\ 0 & 0 \\ 0 & 1 \\ 0 & 0 \end{bmatrix}, \quad \mathbf{U}_{con} = \begin{bmatrix} 0 & 0 \\ 1 & 0 \\ 0 & 0 \\ 0 & 1 \end{bmatrix}, \quad \mathbf{G} = \begin{bmatrix} 1 & 0 & 0 & 0 \\ 1 & 1 & 0 & 0 \\ 0 & 1 & 1 & 0 \\ 0 & 0 & 1 & 1 \end{bmatrix},$$

where the filtering matrix $\mathbf{G}$ implements a low-pass finite impulse response (FIR) filter $\mathbf{g} = [1\ 1]$. From the interpolated tag and control time series, we form a perfusion time series $\mathbf{y}_{perf} = \tilde{\mathbf{y}}_{con} - \tilde{\mathbf{y}}_{tag}$.

The interpolated time series $\mathbf{y}_{perf}$ is an approximation of the perfusion time series that we would obtain if we could simultaneously measure tag and control images. The approximate general linear model is therefore $\mathbf{y}_{perf} \approx \mathbf{X}\mathbf{h}_{perf} + \tilde{\mathbf{S}}\mathbf{b} + \mathbf{n}$, from which we may form an estimate,

$$\tilde{\mathbf{h}}_{perf} = (\mathbf{X}^T\mathbf{P}_{\tilde{\mathbf{S}}}^{\perp}\mathbf{X})^{-1}\mathbf{X}^T\mathbf{P}_{\tilde{\mathbf{S}}}^{\perp}\mathbf{y}_{perf}. \tag{16}$$

For binary stimulus patterns, we show in the Appendix that a very good approximation is

$$\tilde{\mathbf{h}}_{perf} \approx \tilde{\mathbf{G}}\hat{\mathbf{h}}_{perf}, \tag{17}$$

where $\tilde{\mathbf{G}}$ is a $k \times k$ matrix that implements a normalized version of the FIR filter $\mathbf{g}$ that corresponds to the $N \times N$ matrix $\mathbf{G}$. In addition, we require that the frequency response of the filter has zeros at multiples of F_S/M, where $F_S = 1/T_S$ is the sampling frequency of the stimulus pattern, and that the bandwidths of both $\mathbf{X}\mathbf{h}$ and the low-frequency nuisance terms are less than F_S/M.

Equation (17) states that under certain conditions the running subtraction estimate is approximately equal to a filtered version of the direct estimate obtained using the general linear model in Eq. (2). To demonstrate the validity of this approximation and also to show the effect of different downsampling factors and FIR filters, we simulated the estimation process for two experimental designs, both with $T_S = 1$ s. These were a periodic single-trial design with 12 1-s-long events spaced at 21-s intervals and a randomized design with 64 1-s-long events randomly distributed on a 1-s grid over a 256-s interval. Tag and control responses were constructed by convolving the binary stimulus patterns with a gamma density function [Eq. (14)] with parameters $\tau = 1.2$, $n = 3$, $\Delta t = 1$ (Boynton *et al.*, 1996), and $C = -1$ for tag and $C = 2$ for control. In addition, constant offsets of 1000 and 1000.4 were added to the tag and control responses, respectively. The convolved responses were downsampled by a factor of either $M = 2$ or $M = 4$, and direct estimates $\hat{\mathbf{h}}_{perf}$, running subtraction estimates $\tilde{\mathbf{h}}_{perf}$, and filtered direct estimates $\tilde{\mathbf{G}}\hat{\mathbf{h}}_{perf}$ were computed. For the $M = 2$ case, running subtraction and filtered direct estimates were calculated using one of two FIR filters: $\mathbf{g} = [1\ 1]$ or $\mathbf{g} = [1\ 2\ 1]/2$. Note that the filter $\mathbf{g} = [1\ 1]$ is the shortest filter that satisfies the requirement that the FIR filter has zeros in the frequency response at multiples of $F_S/2$ and corresponds to pairwise subtraction of adjacent tag and control images. The filter $\mathbf{g} = [1\ 2\ 1]/2$ places two zeros at each multiple of $F_S/2$ and corresponds to taking the difference of each image from the average of the previous image and the next image as was done in Wong *et al.* (1997). This is also equivalent to linearly interpolating, by a factor of 2, the acquired tag and control time series. For the $M = 4$ case, the estimates were calculated using either $\mathbf{g} = [1\ 1\ 1\ 1]$ or $\mathbf{g} = [1\ 2\ 3\ 4\ 3\ 2\ 1]/4$. The filter $\mathbf{g} = [1\ 1\ 1\ 1]$ is the shortest filter with zeros in the frequency response at multiples of $F_S/4$, while the filter $\mathbf{g} = [1\ 2\ 3\ 4\ 3\ 2\ 1]/4$ places two zeros at each multiple of $F_S/4$ and implements a linear interpolation of the acquired tag and control time series by a factor of 4.

The estimated responses are shown in Figs. 3 and 4. Note that since noise was not included in these simulations, the direct estimate $\hat{\mathbf{h}}_{perf}$ is identical to the ideal

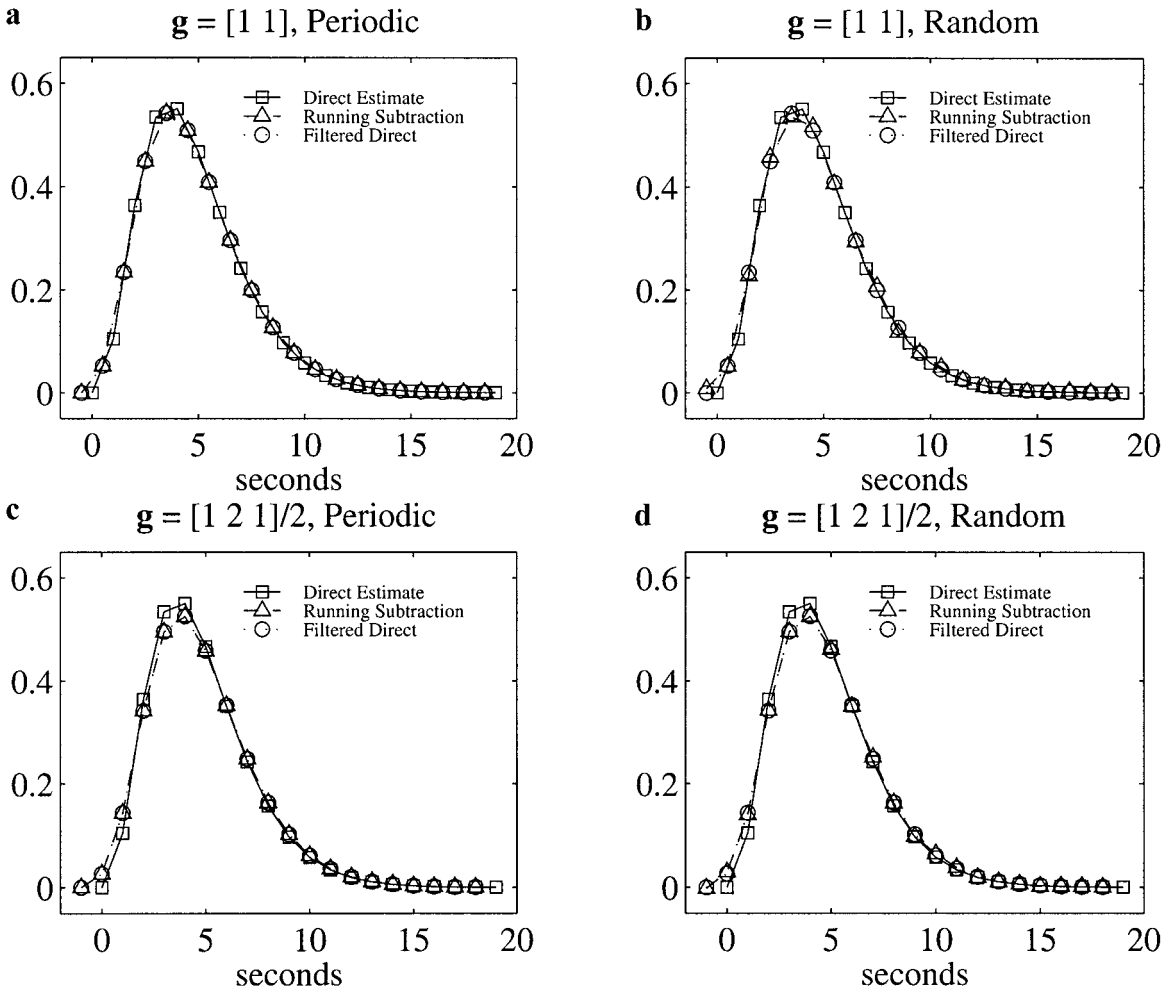

FIG. 3. Perfusion hemodynamic response estimates for periodic and random stimulus patterns and downsampling factor $M = 2$. The "Direct Estimate" is $\hat{\mathbf{h}}_{perf}$, the "Running Subtraction" estimate is $\tilde{\mathbf{h}}_{perf}$, and the "Filtered Direct" estimate is $\tilde{\mathbf{G}}\hat{\mathbf{h}}_{perf}$. FIR filters $\mathbf{g} = [1\ 1]$ and $\mathbf{g} = [1\ 2\ 1]/2$ are used in the top and bottom rows, respectively.

response $\mathbf{h}_{perf}$, which is not shown. The running subtraction estimates and filtered direct estimates have been shifted in time to take into account the delay of the FIR filters used. As an example, with $M = 4$ and $\mathbf{g} = [1\ 1\ 1\ 1]$, the running subtraction estimate is time shifted by 1.5 s with respect to the direct estimate, since the delay of the filter is 1.5 s. For each combination of downsampling factor, filter, and stimulus pattern, the running subtraction estimates show excellent agreement with the filtered direct estimates, thus supporting the validity of the approximation stated in Eq. (17). In each case, the running subtraction estimate shows a decrease in amplitude and a broadening in temporal width compared to the direct estimate, reflecting the effects of the low-pass FIR filter $\mathbf{g}$. For $M = 2$, the full widths at half-maximum (FWHM) of the running subtraction estimates for both the periodic and the randomized designs are 5.0 and 5.1 s for $\mathbf{g} = [1\ 1]$ and $\mathbf{g} = [1\ 2\ 1]/2$, respectively, representing an increase of 0.1 and 0.2 s compared to the 4.9-s FWHM of the direct estimate. For $M = 4$, the FWHM of the running subtraction estimates for the periodic designs are 5.6 and 6.2 s for $\mathbf{g} = [1\ 1\ 1\ 1]$ and $\mathbf{g} = [1\ 2\ 3\ 4\ 3\ 2\ 1]/4$, respectively, representing increases of 0.7 and 1.3 s compared to the direct estimate FWHM. The corresponding FWHM for the randomized designs are slightly smaller and are 5.5 and 6.0 s. Note that the effects of the FIR filter decrease as the bandwidth of the filter increases, so that in practice it is desirable to use the filter with the widest bandwidth possible, e.g., $\mathbf{g} = [1\ 1]$ and $\mathbf{g} = [1\ 1\ 1\ 1]$ for $M = 2$ and $M = 4$, respectively.

As mentioned previously, running subtraction estimates have the potential advantage of reducing the effects of low-frequency drifts and motion-related artifacts. Thus, in experiments with significant artifacts, the running subtraction estimate $\tilde{\mathbf{h}}_{perf}$ may be preferable to the direct estimate $\hat{\mathbf{h}}_{perf}$ if the effects of the FIR

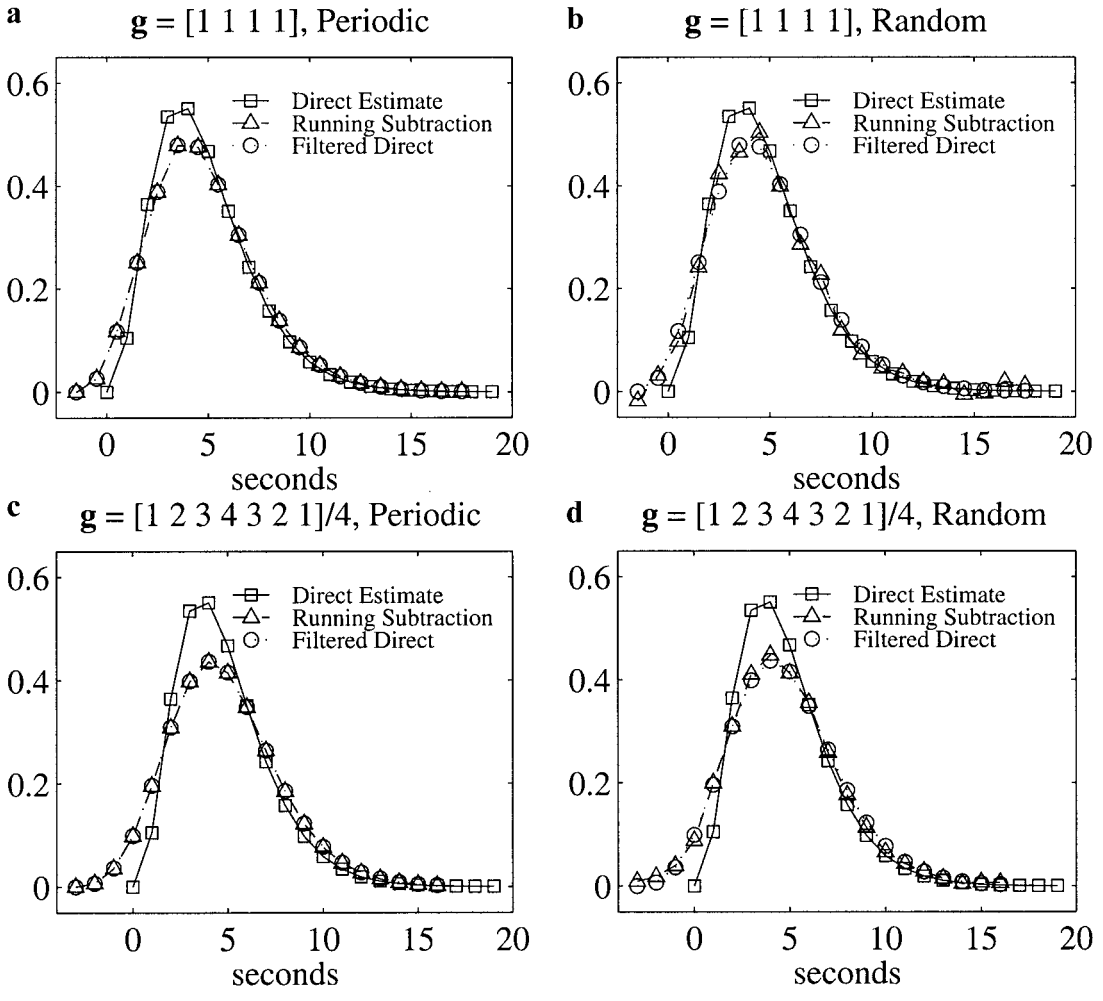

FIG. 4. Perfusion hemodynamic response estimates for periodic and random stimulus patterns and downsampling factor $M = 4$. The "Direct Estimate" is $\hat{\mathbf{h}}_{perf}$, the "Running Subtraction" estimate is $\tilde{\mathbf{h}}_{perf}$, and the "Filtered Direct" estimate is $\tilde{\mathbf{G}}\hat{\mathbf{h}}_{perf}$. FIR filters $\mathbf{g} = [1\ 1\ 1\ 1]$ and $\mathbf{g} = [1\ 2\ 3\ 4\ 3\ 2\ 1]/4$ are used in the top and bottom rows, respectively.

filter are acceptable. As a preliminary test of this hypothesis, we performed a numerical simulation in which a step discontinuity was added to the tag and control time series. These are shown in Figs. 5a and 5b for periodic single-trial and randomized designs, respectively. The ideal response $\mathbf{h}_{perf}$, the direct estimate $\hat{\mathbf{h}}_{perf}$, and the running subtraction estimate $\tilde{\mathbf{h}}_{perf}$ for $M = 4$ and filter $\mathbf{g} = [1\ 1\ 1\ 1]$ are shown in Figs. 5c and 5d. For the periodic design, the direct estimate $\hat{\mathbf{h}}_{perf}$ is severely affected by the discontinuity, while the running subtraction estimate $\tilde{\mathbf{h}}_{perf}$ is much less affected and shows good agreement with the ideal response.

EXPERIMENTAL EXAMPLES

As a preliminary demonstration of the estimation of the perfusion response with different designs, downsampling factors, and analysis methods, we conducted experiments using a periodic single-trial design (24 1-s-long events spaced at 21-s intervals) and a randomized design (128 1-s-long events randomly distributed on a 1-s grid over a 512-s interval). The time resolution T_S is 1 s for both designs. The total length of each experiment (with initial off periods) was 8 min 36 s. Imaging was performed on a 1.5-T GE Signa LX Echospeed system with a standard birdcage headcoil. A PICORE tagging sequence (Wong *et al.*, 1997) with $TR = 2$ s was used to obtain ASL data with a $M = 4$ downsampling factor. A turbo-PICORE tagging sequence (Wong *et al.*, 2000) with $TR = 1$ s was used to obtain ASL data with $M = 2$. For both sequences, the thickness of the tag region was 10 cm and the gap between the tag and the edge of the imaging slice was 1 cm. Readout was performed with a dual-echo single-shot spiral trajectory (Glover, 1999). Other imaging parameters were echo times of 3 and 30 ms, 1100-ms inversion time, 24-cm field of view with a 64×64 matrix. The subject performed sequential finger tap-

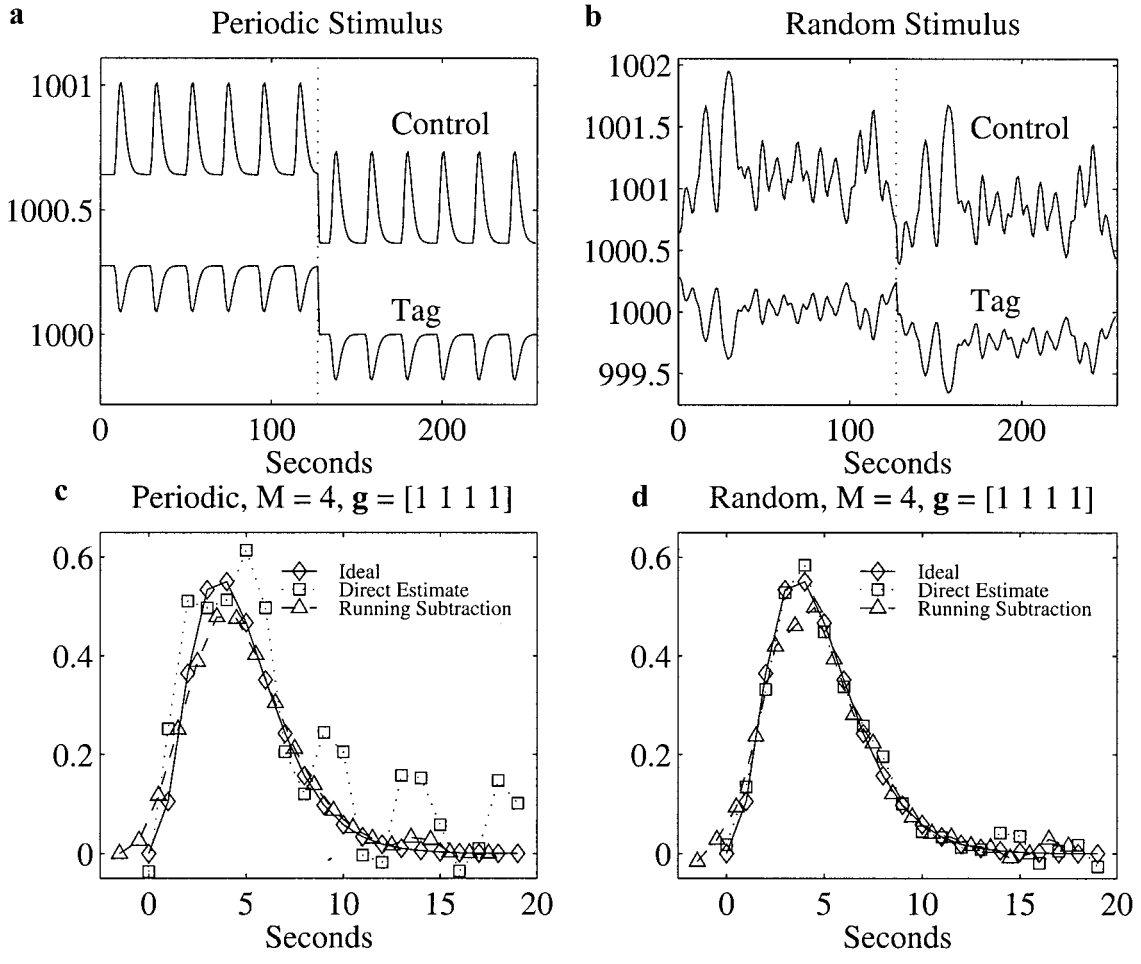

FIG. 5. Simulation of the effect of artifacts on estimates. The tag and control time series for periodic and random stimulus patterns are shown in (a) and (b), respectively, with the vertical dotted lines showing the position of the step discontinuity. The ideal perfusion response and direct and running subtraction estimates with $M = 4$ and $\mathbf{g} = [1\ 1\ 1\ 1]$ are shown in (c) and (d).

ping paced by a flashing checkerboard, and one 8-mm axial slice through the primary motor cortex was imaged.

To select voxels for analysis, a block design run (30 s on/off, four cycles) with turbo-PICORE was performed. Activated voxels were identified by correlating the perfusion time series with a boxcar reference function and thresholding with a correlation coefficient of 0.5. Clustering of the activated voxels was performed by discarding those voxels with fewer than two nearest neighbors. Average time courses were formed for the clustered regions and estimates of the perfusion responses were obtained from the average time courses for the first echo data.

Figure 6 shows direct and running subtraction estimates of the perfusion responses using data from the PICORE and turbo-PICORE experiments. The estimates were calculated using Eqs. (5) and (16), where the dimension of the interference subspace was 4 with Legendre polynomials of order 0 to 3 forming the columns of the matrices $\mathbf{S}$ and $\tilde{\mathbf{S}}$. As was done under Theory, the running subtraction estimates have been shifted in time with respect to the direct estimates to compensate for the delay of the FIR filters used. In agreement with the simulation results, the degree of temporal broadening and reduction in amplitude observed in the running subtraction estimates is much greater in the PICORE estimates compared to the turbo-PICORE estimates, reflecting the smaller bandwidth of the filter used for the PICORE estimates. The amplitudes of the perfusion responses for the randomized design are smaller than those for the periodic single-trial design. This decrease in amplitude is consistent with the presence of neural and hemodynamic nonlinearities (Buxton *et al.*, 2001). Finally, it is important to note that the estimation procedures used here are equally applicable to experiments with other ASL methods. For example, the estimation procedure for a FAIR experiment would be identical to that used here for PICORE.

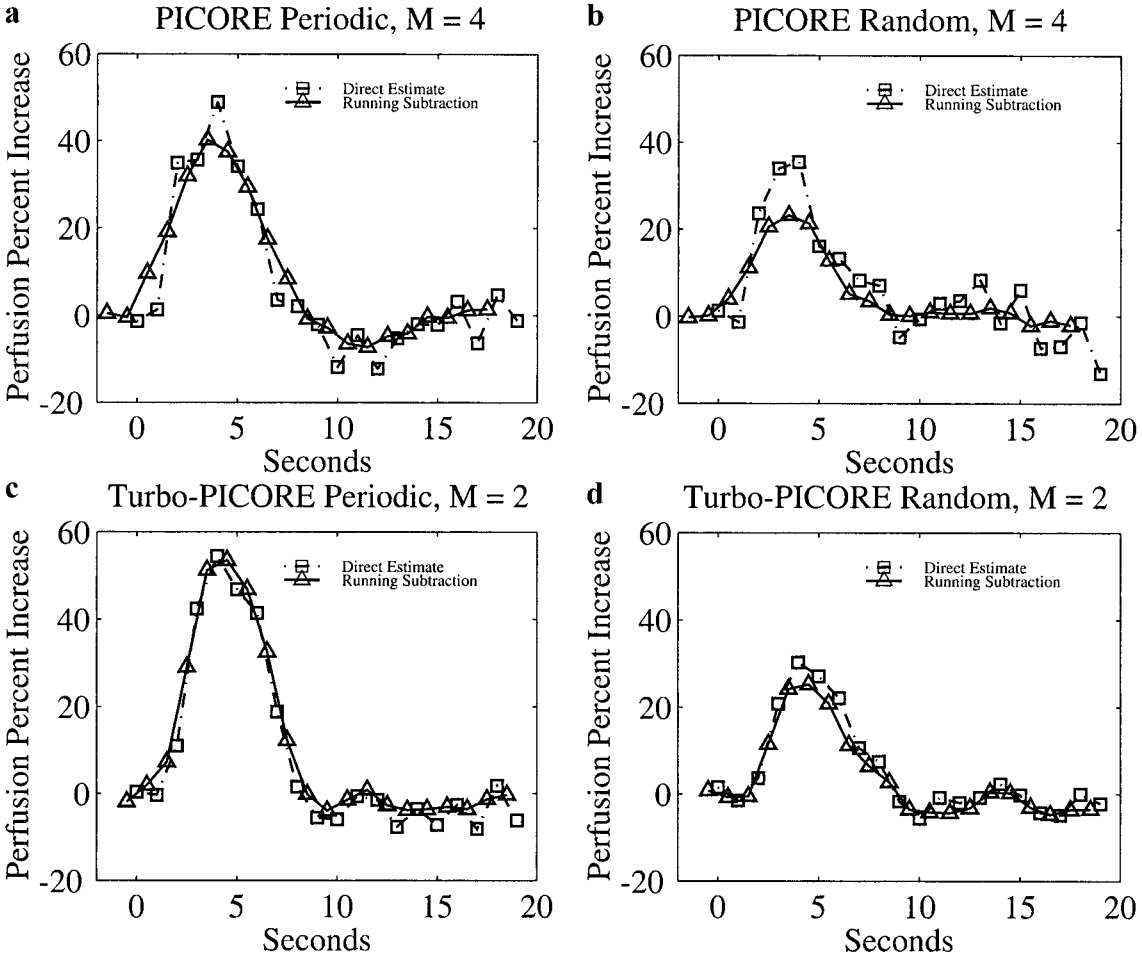

FIG. 6. Direct estimates and running subtraction estimates for PICORE and turbo-PICORE with periodic single-trial and randomized designs. The filters used for the running subtraction estimates are $\mathbf{g}$ = [1 1] for turbo-PICORE and $\mathbf{g}$ = [1 1 1 1] for PICORE.

DISCUSSION AND CONCLUSION

We have presented a general framework for the design and analysis of perfusion-based event-related fMRI experiments. The framework is based on a general linear model in which the interleaving of tag and control images is represented by downsampling matrices. Using this model, we derived exact expressions for the estimate of the perfusion response, an F statistic for detection of the response, and the estimation efficiency and detection power of the experimental design. Of key importance is the fact that these expressions are valid for all designs of interest. Previous treatments have focused on periodic single-trial designs.

The trade-off between estimation efficiency and detection power is an important factor to consider when choosing a design (Liu *et al.*, 2001b). We have derived approximate expressions for efficiency and power that show that the trade-off for perfusion experiments is similar to those previously reported for BOLD experiments. It is important to note that, while these approximate expressions are useful for understanding the nature of the trade-off, the exact expressions [i.e., Eqs. (6) and (11)] should be used whenever selecting a design.

One of the advantages of perfusion experiments is that the interleaving of tag and control images can be useful in reducing the effects of motion-related artifacts since the subtraction of adjacent images removes offsets that are common to both the tag and the control. It has previously been stated that running subtraction approaches are not valid for event-related experiments because they use tag and control images from different time points (Liu and Gao, 1999; Yang *et al.*, 2000). Our theoretical and experimental results show that the running subtraction estimate is a temporally low-pass-filtered version of the direct estimate. The low-pass filtering introduces temporal broadening and a reduction in amplitude of the running subtraction estimate compared to the direct estimate. For some experiments, such as turbo-PICORE with TR = 1 s and M =

2, these effects are small and probably acceptable. For other experiments, such as PICORE with $TR = 2$ s and $M = 4$, the effects are more significant due to the smaller bandwidth of the filter that is required, and the use of the running subtraction estimate should probably be reserved for instances in which the direct estimate is severely degraded by artifacts.

The theoretical framework presented in this paper can be expanded in several areas. First, the framework can be extended to handle noninteger downsampling factors. Rational downsampling factors such that $M = p/q$ where p and q are integers can be accommodated by replacing the downsampling matrices in Eq. (2) with a product of three matrices, where the first matrix upsamples by a factor of q, the second matrix filters the upsampled time series, and the third matrix downsamples by a factor of p (Strang and Nguyen, 1997). Second, we have assumed that the additive noise term $\mathbf{n}$ in Eq. (2) is uncorrelated with covariance $\mathbf{C_n} = \sigma^2\mathbf{I}$. The expressions for estimation efficiency and detection power are readily modified to accommodate the general case in which the covariance matrix is not a multiple of identity, and it would be of interest to see how the structure of the noise covariance affects the trade-off between efficiency and power. In addition, the effect of noise on the running subtraction estimate requires further investigation.

The experimental examples presented here serve as a preliminary demonstration of the application of the theoretical framework. There are a number of interesting experimental questions that are beyond the scope of this paper and could be addressed in future work. In our examples we used turbo-PICORE and PICORE as the ASL methods. A detailed and thorough comparison of the estimates obtained with these two techniques would be useful for understanding how the technical details of an ASL method affect the estimation process. In addition, such a comparison could be extended to other ASL methods, such as FAIR. As stated in Eq. (5), estimates of the BOLD response may also be formed from the experimental data, and it would be of interest to compare the perfusion and BOLD estimates obtained with different ASL methods and stimulus patterns. For example, a detailed study of the reduction in response amplitudes observed for a randomized experiment compared to a periodic single-trial study would be useful in understanding the impact of neural and hemodynamic nonlinearities on the perfusion and BOLD signals.

APPENDIX

We want to show that $\tilde{\mathbf{h}}_{perf} \approx \tilde{\mathbf{G}}\hat{\mathbf{h}}_{perf}$ where $\tilde{\mathbf{h}}_{perf} = (\mathbf{X}^T\mathbf{P}_{\tilde{\mathbf{S}}}^{\perp}\mathbf{X})^{-1}\mathbf{X}^T\mathbf{P}_{\tilde{\mathbf{S}}}^{\perp}\mathbf{G}(\mathbf{U}_{con}\mathbf{y}_{con} - \mathbf{U}_{tag}\mathbf{y}_{tag})$ and $\hat{\mathbf{h}}_{perf} = (\mathbf{X}^T\mathbf{D}_{con}^T\mathbf{P}_{\mathbf{S}}^{\perp}\mathbf{D}_{con}\mathbf{X})^{-1}\mathbf{X}^T\mathbf{D}_{con}^T\mathbf{P}_{\mathbf{S}}^{\perp}\mathbf{y}_{con} - (\mathbf{X}^T\mathbf{D}_{tag}^T\mathbf{P}_{\mathbf{S}}^{\perp}\mathbf{D}_{tag}\mathbf{X})^{-1}\mathbf{X}^T\mathbf{D}_{tag}^T\mathbf{P}_{\mathbf{S}}^{\perp}\mathbf{y}_{tag}$. It is sufficient to derive the approximations $(\mathbf{X}^T\mathbf{P}_{\tilde{\mathbf{S}}}^{\perp}\mathbf{X})^{-1}\mathbf{X}^T\mathbf{P}_{\tilde{\mathbf{S}}}^{\perp}\mathbf{G}\mathbf{U}_{con}\mathbf{y}_{con} \approx \tilde{\mathbf{G}}(\mathbf{X}^T\mathbf{D}_{con}^T\mathbf{P}_{\mathbf{S}}^{\perp}\mathbf{D}_{con}\mathbf{X})^{-1} \times \mathbf{X}^T\mathbf{D}_{con}^T\mathbf{P}_{\mathbf{S}}^{\perp}\mathbf{y}_{con}$ and $(\mathbf{X}^T\mathbf{P}_{\tilde{\mathbf{S}}}^{\perp}\mathbf{X})^{-1}\mathbf{X}^T\mathbf{P}_{\tilde{\mathbf{S}}}^{\perp}\mathbf{G}\mathbf{U}_{tag}\mathbf{y}_{tag} \approx \tilde{\mathbf{G}}(\mathbf{X}^T\mathbf{D}_{tag}^T\mathbf{P}_{\mathbf{S}}^{\perp}\mathbf{D}_{tag}\mathbf{X})^{-1}\mathbf{X}^T\mathbf{D}_{tag}^T\mathbf{P}_{\mathbf{S}}^{\perp}\mathbf{y}_{tag}$. We present here a derivation of the first of these approximations. The derivation of the second is nearly identical. The steps in the derivation are as follows:

$$
\begin{aligned}
&(\mathbf{X}^T\mathbf{P}_{\tilde{\mathbf{S}}}^{\perp}\mathbf{X})^{-1}\mathbf{X}^T\mathbf{P}_{\tilde{\mathbf{S}}}^{\perp}\mathbf{G}\mathbf{U}_{con}\mathbf{y}_{con}\\
&\quad = (\mathbf{X}^T\mathbf{P}_{\tilde{\mathbf{S}}}^{\perp}\mathbf{X})^{-1}\mathbf{X}^T\mathbf{P}_{\tilde{\mathbf{S}}}^{\perp}\mathbf{P}_{\tilde{\mathbf{S}}}^{\perp}\mathbf{G}\mathbf{D}_{con}^T\mathbf{y}_{con}\\
&\quad \approx (\mathbf{X}^T\mathbf{P}_{\tilde{\mathbf{S}}}^{\perp}\mathbf{X})^{-1}\mathbf{X}^T\mathbf{P}_{\tilde{\mathbf{S}}}^{\perp}\mathbf{G}\mathbf{D}_{con}^T\mathbf{P}_{\mathbf{S}}^{\perp}\mathbf{y}_{con}\\
&\quad \approx \tilde{\mathbf{G}}(\mathbf{X}^T\mathbf{P}_{\tilde{\mathbf{S}}}^{\perp}\mathbf{X})^{-1}\mathbf{X}^T\mathbf{P}_{\tilde{\mathbf{S}}}^{\perp}\mathbf{D}_{con}^T\mathbf{P}_{\mathbf{S}}^{\perp}\mathbf{y}_{con}\\
&\quad \approx \tilde{\mathbf{G}}(\mathbf{X}^T\mathbf{D}_{con}^T\mathbf{P}_{\tilde{\mathbf{S}}}^{\perp}\mathbf{D}_{con}\mathbf{X})^{-1}\mathbf{X}^T\mathbf{D}_{con}^T\mathbf{P}_{\mathbf{S}}^{\perp}\mathbf{y}_{con}.
\end{aligned}
$$

The first step is based on the identities $\mathbf{U}_{con} = \mathbf{D}_{con}^T$ and $\mathbf{P}_{\tilde{\mathbf{S}}}^{\perp} = \mathbf{P}_{\tilde{\mathbf{S}}}^{\perp}\mathbf{P}_{\tilde{\mathbf{S}}}^{\perp}$. The second step is valid if the approximations (a) $\mathbf{P}_{\tilde{\mathbf{S}}}^{\perp}\mathbf{G}\mathbf{D}_{con}^T\mathbf{D}_{con}\mathbf{X}\mathbf{h} \approx \mathbf{G}\mathbf{D}_{con}^T\mathbf{P}_{\mathbf{S}}^{\perp}\mathbf{D}_{con}\mathbf{X}\mathbf{h}$ and (b) $\mathbf{P}_{\tilde{\mathbf{S}}}^{\perp}\mathbf{G}\mathbf{D}_{con}^T\mathbf{S}\mathbf{b}_{con} \approx \mathbf{0}$ are reasonable. One requirement for both approximations to hold is that the nuisance terms are limited to low-frequency components (i.e., a constant term and low-frequency drift terms). Approximation (b) holds in this case because both $\mathbf{P}_{\tilde{\mathbf{S}}}^{\perp}$ and $\mathbf{P}_{\mathbf{S}}^{\perp}$ remove only very low-frequency terms and do not greatly affect the replicated frequency domain images of $\mathbf{D}_{con}\mathbf{X}\mathbf{h}$, which are at multiples of F_S/M. In addition the bandwidth of $\mathbf{X}\mathbf{h}$ should be less than F_S/M. This is true for most designs of interest and typically encountered hemodynamic responses (typical full width at half-maximum bandwidth of about 0.1 Hz). As an example, in an experiment which lasts for 120 s with F_S equal to 1 Hz and $M = 4$, the lowest frequency domain image will be centered at 0.25 Hz and the nuisance terms will have frequencies below about 0.017 Hz (e.g., allowing for a nuisance term with two cycles within the 120 s). In order for approximation (b) to hold an additional requirement is that the frequency response of the filter implemented by $\mathbf{G}$ has zeros at multiples of F_S/M. For example, for $M = 4$, the approximation is valid for a filter with coefficients [1 2 3 4 3 2 1]/4 but not for a filter with coefficients [1 4 8 10 8 4 1]/10. These nulls in the frequency response are critical in removing the usually large constant term that is replicated in the frequency domain at multiples of F_S/M by the downsampling process. The third step relies on the fact that $\mathbf{G}$ implements an interpolation filter and $(\mathbf{X}^T\mathbf{P}_{\tilde{\mathbf{S}}}^{\perp}\mathbf{X})^{-1}\mathbf{X}^T\mathbf{P}_{\tilde{\mathbf{S}}}^{\perp}$ may also be viewed as a filtering matrix since it deconvolves the effects of the experimental stimulus pattern. Because filtering is a commutative operation, we can use the approximation $(\mathbf{X}^T\mathbf{P}_{\tilde{\mathbf{S}}}^{\perp}\mathbf{X})^{-1}\mathbf{X}^T\mathbf{P}_{\tilde{\mathbf{S}}}^{\perp}\mathbf{G} \approx \tilde{\mathbf{G}}(\mathbf{X}^T\mathbf{P}_{\tilde{\mathbf{S}}}^{\perp}\mathbf{X})^{-1}\mathbf{X}^T\mathbf{P}_{\tilde{\mathbf{S}}}^{\perp}$ where $\tilde{\mathbf{G}}$ implements the same filter as $\mathbf{G}$ with appropriately modified dimensions. In addition, the coefficients of $\tilde{\mathbf{G}}$ are normalized so that the gains at zero frequency of $\tilde{\mathbf{G}}$ and

$\mathbf{D}_{con}\mathbf{G}$ are identical. The final step makes use of the approximation in Eq. (12) and the approximation $\mathbf{P}_{\mathbf{S}}^{\perp}\mathbf{D}_{con}^{T}\mathbf{P}_{\mathbf{S}}^{\perp}\mathbf{D}_{con}\mathbf{Xh} \approx \mathbf{D}_{con}^{T}\mathbf{P}_{\mathbf{S}}^{\perp}\mathbf{D}_{con}\mathbf{Xh}$. The justification for this last approximation is similar to that for approximation (a) in step 2.

ACKNOWLEDGMENTS

This work was supported by Grants NINDS-36722 and NINDS-36211 from the National Institutes of Health and Merit Review Award SA321 from the Veterans Administration. We thank Karam Sidaros for helpful discussions.

REFERENCES

Behrens, R. T., and Scharf, L. L. 1994. Signal processing applications of oblique projection operators. *IEEE Trans. Signal Process.* **42:** 1413–1424.

Boynton, G. M., Engle, S. A., Glover, G. H., and Heeger, D. J. 1996. Linear systems analysis of functional magnetic resonance imaging in human V1. *J. Neurosci.* **16:** 4207–4221.

Buxton, R. B., Liu, T. T., Martinez, A., Frank, L. R., Luh, W.-M., and Wong, E. C. 2000. Sorting out event-related paradigms in fMRI: The distinction between detecting an activation and estimating the hemodynamic response. *NeuroImage* **11:** S457.

Buxton, R. B., Liu, T. T., and Wong, E. C. 2001. Nonlinearity of the hemodynamic response: Modeling the neural and BOLD contributions. In *Proceedings of the 9th ISMRM Meeting. Glasgow, Scotland,* p. 1164.

Dale, A. M. 1999. Optimal experimental design for event-related fMRI. *Hum. Brain Mapp.* **8:** 109–114.

Duong, T. Q., Kim, D.-S., and Kim, S. G. 2000. Simultaneous CBF and BOLD fMRI of the cat visual cortex: Comparison of spatial specificity at sub-millimeter resolution. In *Proceedings of the 8th Meeting, International Society for Magnetic Resonance in Medicine, Denver, CO,* p. 980.

Friston, K. J., Holmes, A. P., Worsley, K. J., Poline, J.-P., Frith, C. D., and Frackowiak, R. S. J. 1995. Statistical parametric maps in functional imaging: A general linear approach. *Hum. Brain Mapp.* **2:** 189–210.

Friston, K. J., Zarahn, E., Josephs, O., Henson, R. N. A., and Dale, A. M. 1999. Stochastic designs in event-related fMRI. *NeuroImage* **10:** 607–619.

Glover, G. H. 1999. Simple analytic spiral k-space algorithm. *Magn. Reson. Med.* **42:** 412–415.

Liu, H.-L., and Gao, J.-H. 1999. Perfusion-based event-related fMRI. *Magn. Reson. Med.* **42:** 1011–1013.

Liu, T. T., Frank, L. R., Wong, E. C., and Buxton, R. B. 2001a. Are semi-random designs better than random designs for event-related fMRI? In *Proceedings of the 9th Annual ISMRM Meeting, Glasgow, Scotland,* p. 1707.

Liu, T. T., Frank, L. R., Wong, E. C., and Buxton, R. B. 2001b. Detection power, estimation efficiency, and predictability in event-related fMRI. *NeuroImage* **13:** 759–773.

Liu, T. T., Wong, E. C., Sidaros, K., Frank, L. R., and Buxton, R. B. 2001c. Event-related perfusion fMRI with randomized designs. In *Proceedings of the 9th ISMRM Meeting, Glasgow, Scotland,* p. 1212.

Luh, W. M., Wong, E. C., Bandettini, P. A., Ward, B. D., and Hyde, J. S. 2000. Comparison of simultaneously measured perfusion and BOLD signal increases during brain activation with T1-based tissue identification. *Magn. Reson. Med.* **44:** 137–143.

Miller, K. L., Luh, W.-M., Liu, T. T., Martinez, A., Obata, T., Wong, E. C., Frank, L. R., and Buxton, R. B. 2000. Characterizing the dynamic perfusion response to stimuli of short duration. In *Proceedings of the Eighth Meeting, International Society for Magnetic Resonance in Medicine, Denver, CO,* p. 500.

Rosen, B. R., Buckner, R. L., and Dale, A. M. 1998. Event-related functional MRI: Past, present, and future. *Proc. Natl. Acad. Sci. USA* **95:** 773–780.

Scharf, L. L. 1991. *Statistical Signal Processing: Detection, Estimation, and Time Series Analysis.* Addison–Wesley, Reading, MA.

Seber, G. A. F. 1977. *Linear Regression Analysis.* Wiley, New York.

Strang, G., and Nguyen, T. 1997. *Wavelets and Filter Banks.* Wellesley–Cambridge Press, Cambridge, MA.

Wong, E. C., Buxton, R. B., and Frank, L. R. 1997. Implementation of quantitative perfusion imaging techniques for functional brain mapping using pulsed arterial spin labeling. *NMR Biomed.* **10:** 237–249.

Wong, E. C., Liu, T. T., Frank, L. R., and Buxton, R. B. 2001. Close tag, short TR continuous ASL for functional brain mapping: High temporal resolution ASL with a BOLD sized signal at 1.5T. In *Proceedings of the Ninth Meeting, International Society for Magnetic Resonance in Medicine, Glasgow, Scotland,* p. 1162.

Wong, E. C., Luh, W.-M., and Liu, T. T. 2000. Turbo ASL: Arterial spin labeling with higher SNR and temporal resolution. *Magn. Reson. Med.* **44:** 511–515.

Yang, Y., Engelien, W., Pan, H., Xu, S., Silbersweig, D. A., and Stern, E. 2000. A CBF-based event-related brain activation paradigm: Characterization of impulse–response function and comparison to BOLD. *NeuroImage* **12:** 287–297.